

# Calculations of Higher Multipole Components in a Large Superconducting Quadrupole Magnet

J. Napolitano and T. Hunter

*Physics Division, CEBAF, Newport News, VA 23606*

November 30, 1990

## Abstract

We analyze the magnetic field of a finite length, large bore superconducting quadrupole magnet for use in a large aperture, high momentum magnetic spectrometer. In particular, we study the 12-pole and 20-pole components which would contribute to geometric aberrations. The magnet is 130 *cm* long, has a pole radius of 43 *cm*, and the field is largely iron dominated. We analyze the magnet with a nominal field gradient of 276 *gauss/cm*. The field and/or the scalar potential is calculated with the program TOSCA and decomposed consistent with magnetostatic theory. We establish that the small multipole components are determined reliably and consistently. We find that although the absolute magnitude of the higher order multipoles can become quite large near the ends of the magnet, they reverse sign in this region and their contributions to the field integral are quite small. At the pole radius the integral contributions of the 12-pole ( $n = 6$ ) and 20-pole ( $n = 10$ ) are  $\approx 1.2 \times 10^{-2}$  and  $\approx 2.4 \times 10^{-3}$  respectively, relative to the quadrupole ( $n = 2$ ). We estimate the errors in these values due to uncertainties in the numerical calculations to be  $\approx \pm 5\%$  and  $\approx \pm 20\%$  respectively.

# 1 Introduction

Superconducting magnet technology has made it possible to achieve large fields and field gradients over substantial volumes. Focussing magnetic spectrometers which accept large phase space regions are being designed using this technology. The large acceptance is achieved using quadrupole magnets which ideally focus parallel monochromatic rays to the same point. In such an ideal quadrupole, the transverse magnetic field intensity is proportional to the distance  $r$  from the axis of the magnet [1]. Higher order multipoles spoil this radial field dependence and lead to geometric aberrations in the final instrument. In general, then, one wants to minimize the contributions of these higher order multipoles to the field.

We have studied the design of one such quadrupole magnet in detail. The design [2] is based on a conformal mapping of a window frame dipole magnet to a quadrupole geometry. A cross section of the magnet is shown in Fig. 1. A strict conformal mapping implies hyperbolic pole tips and coil windings, as well as a hyperbolic current density. Although it is straightforward to construct hyperbolic pole tip shapes, it is difficult in practice to achieve a hyperbolic current distribution. To simplify the construction, the coils are wound into flat sheets (carrying constant current density) and tilted at an angle of  $5^\circ$  with respect to the centerline to approximate the effect of hyperbolic shape and current density. The pole tip radius is 43 *cm* and the maximum useful radius is 38 *cm*. The iron is 130 *cm* long and has no shaping at the ends.

Such a magnet offers many attractive advantages over other large bore, high gradient designs such as the “ $\cos 2\theta$ ” [3] and “Panofsky” [4] options. These include good gradient uniformity over a large fraction of the useful bore, and relative ease of construction and low cost. However, the compromise coil design and the finite length (including the coil return at the ends) may introduce significant higher order multipoles to the field, even with ideal

placement of all components. Until now, this magnet had only been studied using two dimensional magnetostatics codes such as POISSON. In this paper, we describe the results of a three dimensional analysis using the code TOSCA. Included are a number of checks that the results are consistent over a range of assumptions, and that the numerical solutions are consistent with Laplace's equation, even for the small multipole components.

The remainder of this paper presents the results of our study. First, we outline the formalism of the solution to Laplace's equation in cylindrical coordinates with particular emphasis on higher order multipoles. Second, we show details of the three dimensional magnetic field calculation using the programs TOSCA and VF/OPERA. Finally we show the results for the various multipole components, and tabulate their integrals over  $z$ . The instrument for which this magnet was designed (the CEBAF High Momentum Spectrometer) requires an  $n = 6$  multipole contribution of less than 3% extrapolated to the pole tip [5]. We conclude that this condition can certainly be met using magnets of this type.

## 2 Formalism

The magnetic field  $\vec{B}$  in free space may be described in terms of a scalar potential  $\Phi$  as  $\vec{B} = \vec{\nabla}\Phi$ , where we neglect an irrelevant overall sign. The scalar potential  $\Phi$  solves Laplace's equation, namely

$$\nabla^2\Phi = \frac{1}{r} \frac{\partial}{\partial r} \left( r \frac{\partial\Phi}{\partial r} \right) + \frac{1}{r^2} \frac{\partial^2\Phi}{\partial\theta^2} + \frac{\partial^2\Phi}{\partial z^2} = 0 \quad (1)$$

We use cylindrical coordinates since they are most suitable for quadrupole magnet geometries. There are an infinite number of solutions which, apart from an arbitrary angular phase and assuming that  $z = 0$  is the center of the magnet, may be written as [6]

$$\Phi^{(n,k)}(r, \theta, z) = \text{Normalization} \cdot \cos n\theta e^{\pm kz} J_n(kr) \quad (k \neq 0)$$

where

$$J_n(x) = \left(\frac{x}{2}\right)^n \sum_{m=0}^{\infty} \frac{(-1)^m}{m! \Gamma(m+n+1)} \left(\frac{x}{2}\right)^{2m}$$

is a Bessel function of order  $n$ . (If  $k = 0$ , then there is no dependence on  $z$  and  $\Phi$  is simply proportional to  $\cos n\theta \cdot r^n$ .) The values of  $n$  and  $k$  are in principle arbitrary, although  $n$  must be an integer if the potential is to be single valued. In a problem with eight-fold symmetry (like the one we consider here) the radial component of the field,  $B_r(r, \theta, z) = \partial\Phi/\partial r$ , reverses sign from  $\theta = 0$  to  $\theta = \pi/2$  and we must have  $n = 2, 6, 10, \dots$  only. For a finite length magnet any  $k \neq 0$  solution is in principle allowed. Note that the solution must also be symmetric between  $z$  and  $-z$ .

The correct linear combination of the above solutions is determined by applying boundary conditions. These boundary conditions depend on the placement of iron and currents, as well as the behavior as  $z \rightarrow \infty$ . The general solution then has the following form [7]:

$$\begin{aligned} \Phi(r, \theta, z) &= \sum_{n=0}^{\infty} \cos n\theta \Phi_n(r, z) \\ &= \sum_{n=0}^{\infty} \left( \cos n\theta \left(\frac{r}{r_0}\right)^n \sum_{m=0}^{\infty} \left[ \bar{b}_{m,n}(z) \left(\frac{r}{r_0}\right)^{2m} \right] \right) \end{aligned} \quad (2)$$

and the radial field is

$$\begin{aligned} B_r(r, \theta, z) = \frac{\partial\Phi}{\partial r} &= \sum_{n=0}^{\infty} \cos n\theta B_{r,n}(r, z) \\ &= \sum_{n=0}^{\infty} \left( \cos n\theta \left(\frac{r}{r_0}\right)^{n-1} \sum_{m=0}^{\infty} \left[ b_{m,n}(z) \left(\frac{r}{r_0}\right)^{2m} \right] \right) \end{aligned} \quad (3)$$

where

$$\bar{b}_{m,n}(z) = b_{m,n}(z) \frac{r_0}{2m+n} \quad (4)$$

and the scale radius  $r_0$  (generally chosen to be the pole radius) ensures that the  $b_{m,n}$  all have the units of magnetic field. The dependence on  $r$  is dictated by the behavior of the Bessel function  $J_n(kr)$ .

The  $b_{m,n}$  are constructed from the expansion of the  $e^{\pm kz}$  which meets the boundary conditions. Constraints on them are derived from symmetry

and by insisting that  $\Phi$  solve Laplace's equation. We substitute Eqn. 2 and Eqn. 4 into Eqn. 1 and use the orthogonality of the  $\cos n\theta$  to treat the terms in  $n$  separately. We arrive at the following recursion relation for the  $b_{m,n}(z)$ :

$$b_{m,n}(z) = \frac{2m+n}{4m(m+n)(2m+n-2)} r_0^2 \frac{d^2 b_{m-1,n}}{dz^2} \quad \text{for } m \geq 1 \quad (5)$$

Also, since the  $z$ -component of the field,  $B_z(r, \theta, z)$ , must vanish at  $z = 0$  and as  $z \rightarrow \infty$ , we can show that

$$\frac{db_{m,n}}{dz} = 0 \text{ at } z = 0 \text{ and } z \rightarrow \infty \quad (6)$$

The behavior of a spectrometer is determined mainly by the integrals of the field components over  $z$ . That is,

$$\int_0^\infty B_{r,n}(r, z) dz = \left(\frac{r}{r_0}\right)^{n-1} \sum_{m=0}^\infty \left(\frac{r}{r_0}\right)^{2m} \int_0^\infty b_{m,n}(z) dz$$

However, using Eqn. 5 and Eqn. 6 it is easy to show that only the  $m = 0$  term contributes. Hence,

$$\int_0^\infty B_{r,n}(r, z) dz = \left(\frac{r}{r_0}\right)^{n-1} \int_0^\infty b_{0,n}(z) dz \quad (7)$$

That is, in determining the integral of the multipole, only the leading term in the radial expansion is important. Equation 7 also shows that the integral must be proportional to  $r^{n-1}$ .

In practice, one uses a three dimensional numerical integration program to calculate the scalar potential and/or the magnetic fields. (For this work, we use the program TOSCA [8].) The individual multipole components (specified by the value of  $n$ ) are extracted using a straightforward Fourier analysis, for fixed radii  $r$  and axial positions  $z$ . These data are then fit as a function of  $r$  for the different values of  $z$  to determine the coefficients  $b_{m,n}(z)$  or  $\bar{b}_{m,n}(z)$ . These in turn determine the magnetic field.

Note that determining  $b_{m,n}$  may be difficult for large  $n$  since they multiply large powers of  $r$  and are determined primarily by the behavior close

to the pole tip. Numerical programs which calculate the magnetic field by some finite difference method solution of Eqn. 1 cannot be expected to give highly reliable results near the interface of a vacuum and a highly nonlinear material such as the iron pole tip. However, since the field integrals depend only on the coefficients  $b_{0,n}$  it is possible to determine these at lower radii (where they dominate over the other  $b_{m,n}$ ) and extrapolate to  $r = r_0$ .

### 3 TOSCA calculation

The program TOSCA computes (among other things) three dimensional magnetic fields in the presence of arbitrary current distributions including the presence of nonlinear materials [8]. In regions of space where the current density is zero, the magnetic field may be defined in terms of a scalar potential which solves Laplace's equation. In regions where currents are present, the program calculates the magnetic field directly using the Biot-Savart law. We note that TOSCA has been used to analyze quadrupole magnets and the results have been compared to measurement [9].

As we shall see, the net contribution from higher order multipoles after integrating along  $z$  results from the cancellation of relatively large terms of opposite sign. Also, these higher order multipoles may be small fractions of the dominant quadrupole. Consequently, we want to be able to check the calculation using as many variants as possible. We take care to configure the problem so that the interior of the magnet is recognized to be a current-free region everywhere. This allows us to compare the results from the scalar potential and from the magnetic field directly. Indeed, when configured so that part of the field was calculated directly and the rest using the "reduced" scalar potential, we have seen that the individual multipoles do not tend to zero at large  $z$  rendering the integrals meaningless.

The mesh used in the  $r\theta$  plane of the magnet is shown in Fig. 2. Eightfold symmetry is assumed. Boundary conditions are  $\Phi = \text{constant}$  along the

horizontal and vertical edges, and  $B_{normal} = 0$  along the symmetry edge running through the center of the pole face. This mesh is replicated in  $z$  with the granularity shown in Table 1. This results in a total of 31,000 mesh points. The magnet iron ends abruptly at  $z = 65$  cm with no shaping or chamfer. The coils are wound in a Bedstead-type geometry shown in Fig. 3. The problem takes roughly 5 hrs of CPU time on a VAX-8700 undergoing 15 iterations.

The boundary conditions as  $z \rightarrow \infty$  must also be specified. We specify these boundary conditions as either  $\Phi = constant$  or as  $\partial\Phi/\partial z = 0$ . Note that “ $\infty$ ” is simply the longitudinal extent of the problem (which is kept to a minimum to avoid excess computer time). For this analysis the  $z \rightarrow \infty$  boundary condition is defined at  $z = 170$  cm.

## 4 Multipole analysis

The post-process program VF/OPERA [8] Fourier analyzes  $B_r(\theta)$  or  $\Phi(\theta)$ . We calculate both  $B_r$  and  $\Phi$  using each of the two boundary conditions at  $z \rightarrow \infty$  (i.e.  $\Phi = constant$  and  $\partial\Phi/\partial z = 0$ ) giving us a total of four data sets. Each data set consists of the extracted multipole, either  $\Phi_n(r, z)$  or  $B_{r,n}(r, z)$ , tabulated at various values of  $z$  and  $r$ . Values of  $z$  run between 0 and 170 cm (with points closest together in the region near the end of the magnet iron). Values of  $r$  are in 4 cm steps between 2 and 34 cm, in 2 cm steps up to 40 cm, and an additional point at 41 cm. (Recall that the pole radius is 43 cm.) A typical VF/OPERA run takes  $\approx 3$  hr of CPU time on a VAX-8700.

The radial dependence of each multipole component is fit to the form described in Eqn. 2 or Eqn. 3 to determine the parameters  $\bar{b}_{m,n}$  or  $b_{m,n}$ . Each data point is weighted equally. Four terms corresponding to  $m = 0, 1, 2,$  and  $3$  are included. When fitting  $\Phi_n(r)$ , we use Eqn. 4 to determine coefficients for  $B_{r,n}(r)$ . This should in principle be more precise than fitting

$B_{r,n}(r)$  directly since we do not rely on the result of a numerical derivative. That is, we take an analytic derivative of  $\Phi_n(r)$  having determined the coefficients.

Figure 4 shows fits to  $B_{r,n}(r, z)$  at  $z = 0$  (with  $\Phi = \text{constant}$  boundary conditions) for  $n = 2, 6,$  and  $10$ . Other multipole components (for  $n < 14$ ) are consistent with zero, as they must be from symmetry considerations. Figure 5 shows the same information at  $z = 70 \text{ cm}$ . In all cases, the TOSCA calculations are well-described by Eqn. 3. In the cases for  $z = 70 \text{ cm}$  it is also clear that the lowest order radial dependence (i.e.  $m = 0$  only) is not sufficient to describe the data.

Let us now consider the behavior of the different  $n$  components of the radial field as a function of the longitudinal position  $z$ . We start by considering the (dominant)  $n = 2$  component. Figure 6 shows the coefficients  $b_{0,2}$ ,  $b_{1,2}$ ,  $b_{2,2}$  and  $b_{3,2}$  as a function of  $z$ , obtained by fitting the data as described above. The radial field component at the pole tip, i.e.  $B_{r,2}(r = r_0 = 43 \text{ cm}, z)$  determined by the fitted coefficients, is also shown. As suggested in Figs. 4 and 5, the fit is dominated by the lowest order (i.e.  $m = 0$ ) coefficient in the interior of the magnet, but near the end of the magnet iron and beyond there is a large contribution from higher orders. Equation 7 says that the area under the  $b_{0,2}(z)$  curve is the same as that under the  $B_{r,2}(r_0, z)$  curve, while the other  $b_{m,2}(z)$  integrate to zero.

Equation 5 may be directly tested at this point. Figure 7 compares  $b_{1,2}(z)$  and  $(r_0^2/6)d^2b_{0,2}/dz^2$  which should be the same according to Eqn 5. The agreement is very good, demonstrating a level of internal consistency in our procedure so far.

Next we discuss the  $n = 2$  field components  $B_{r,2}(r, z)$  as determined from our fits. These are plotted as a function of  $z$  for  $r = r_0 = 43 \text{ cm}, 38 \text{ cm},$  and  $30 \text{ cm}$  in Fig. 8. We also plot the integrals of these functions, integrated up to the plotted value of  $z$ , to show their development

and convergence. There is a rather long tail to large  $z$ , but the contribution to the integral past  $z \approx 120 \text{ cm}$  is rather small.

Finally, we show in figures 9 and 10 the field components for  $n = 6$  and  $n = 10$  respectively, plotted in the same way as the  $n = 2$  results in Fig. 8. Note that these components change sign in the region near the end of the magnet iron, and there is a significant cancellation in the final field integral. We note that these functions are qualitatively very similar to those obtained in magnetic field measurements of actual quadrupole magnets [10].

Table 2 summarizes the results of the integrated multipoles for our four data sets (i.e. using Eqn. 2 or Eqn. 3 with either of the two types of boundary conditions). Our goal here is to identify reasonable and consistent values for the multipole field integrals in the face of the limitations of the numerical calculations and of the large cancellations near the end of the magnet iron. Listed are the multipole components integrated from  $0 \leq z \leq 170 \text{ cm}$ . For  $n = 2$  we list the field integral in  $T \cdot m$ , and for  $n = 6$  and  $n = 10$  we list the ratio (%) to the corresponding  $n = 2$  integral. For each multipole and data type, we tabulate the integral of  $b_{0,n}$  and of the radial field at radii  $r = 43 \text{ cm}$  (the pole tip radius),  $r = 38 \text{ cm}$  (the maximum useful radius of the magnet), and  $r = 30 \text{ cm}$ . For each data set the radial fits are performed twice; once using all data and once restricting the data to  $r \leq 38 \text{ cm}$ .

Notice first that all results are rather insensitive to the choice of boundary condition (i.e.  $\Phi = \text{constant}$  or  $\partial\Phi/\partial z = 0$ ) used to solve the problem. This is an important consistency check. As the differences are relatively small, we will not try to argue which should be more appropriate. Note also that the results for  $n = 2$  always satisfy Eqn. 7.

We have suggested that fitting  $\Phi_n(r)$  and using Eqn. 4 to determine the  $b_{m,n}$ , rather than fitting  $B_{r,n}(r)$  directly, should be more precise. That is supported by Table 2. In particular, for  $n = 6$  the integral of  $b_{0,6}$  is somewhat more consistent with the integral of  $B_{r,6}(r = r_0 = 43 \text{ cm})$  when fitting  $\Phi_6(r)$ .

More pointedly, for  $n = 10$  the integral of  $B_{r,10}(r = r_0 = 43 \text{ cm})$  is consistent with Eqn. 7 and the integrals of  $B_{r,10}(r)$  at  $r = 38 \text{ cm}$  and at  $r = 30 \text{ cm}$  *only* for the data sets that fit  $\Phi_{10}(r)$ . Indeed, even the sign is incorrect when fitting  $B_{r,10}(r)$ . (Note that the ratio of the integral for multipole  $n$  to that for  $n = 2$  goes like  $(r/r_0)^{n-2}$  according to Eqn. 7.)

We also suggest above that the results of TOSCA calculations may be suspect for radii very close to the pole tip, i.e.  $r \approx r_0 = 43 \text{ cm}$ . This is unfortunate since we want to determine the field integrals at  $r = r_0$ . However, if we can reliably determine the field integrals at smaller radii, we can use Eqn. 7 to extrapolate to the pole radius. Table 2 shows the field integrals obtained by fitting all radial data, and also by only fitting data with  $r \leq 38 \text{ cm}$ . For both  $n = 6$  and  $n = 10$ , consider the four field integrals at  $r = 30 \text{ cm}$  obtained by fitting  $\Phi_n(r)$  for each of the two boundary conditions, and for fitting all data or just  $r \leq 38 \text{ cm}$ . The results for  $n = 6$  (-0.26% to -0.28%) and for  $n = 10$  (0.013% to 0.015%) are quite consistent. This is also true for the  $n = 6$  at  $r = 38 \text{ cm}$  and, to a lesser extent, the  $n = 10$  at  $r = 38 \text{ cm}$ .

Now we use the fits to  $\Phi_n(r)$  to determine the integrated multipoles at  $r = r_0$ . We use both the results at  $r = 30 \text{ cm}$  and  $r = 38 \text{ cm}$  (a total of eight evaluated field integrals for each multipole), in conjunction with Eqn. 7, to determine the field integrals at  $r = r_0 = 43 \text{ cm}$  for  $n = 6$  and  $n = 10$ . We average over the eight results. Including the integrated quadrupole ( $n = 2$ ) component, we summarize our results as follows:

$$\begin{aligned} \frac{1}{2} \int_{-\infty}^{\infty} B_{r,2}(43 \text{ cm}, z) dz &= \int_0^{\infty} B_{r,2}(43 \text{ cm}, z) dz = 0.94 T \cdot m \\ \int_0^{\infty} B_{r,6}(43 \text{ cm}, z) dz &= (-1.2 \times 10^{-2}) \times 0.94 T \cdot m \\ \int_0^{\infty} B_{r,10}(43 \text{ cm}, z) dz &= (2.4 \times 10^{-3}) \times 0.94 T \cdot m \end{aligned}$$

The eight extrapolated values for  $n = 6$  range from  $1.1 \times 10^{-2}$  to  $1.2 \times 10^{-2}$  so we estimate the precision of the final answer to be roughly  $\pm 5\%$ . The eight values for  $n = 10$  range from  $1.8 \times 10^{-3}$  to  $2.8 \times 10^{-3}$  so we estimate

the precision in this case to be roughly  $\pm 20\%$ .

We note that these should meet the design specifications [5] of  $\leq 3 \times 10^{-2}$  for  $n = 6$  (assuming it is known) and  $\leq 3 \times 10^{-3}$  for unknown multipoles in general. Furthermore, there has been no attempt to optimize the design by either shaping the ends of the iron or by adding small “correction coils” within the cryostat. Given the understanding of TOSCA demonstrated here, such modifications to the design should be relatively straightforward.

## 5 Acknowledgements

We are particularly indebted to Dr. L. Harwood for suggesting this method of analysis and for many useful conversations during the course of this work. Comments and cross checks were provided by S. Lassiter. Finally, we acknowledge general support and encouragement from Dr. L. Cardman and Dr. R. Carlini. This work was supported by the U.S. Department of Energy under contract number DE-AC05-84ER40150.

## References

- [1] E.Reigenstreif, "Focusing with Quadrupoles, Doublets, and Triplets", in *Focusing with Charged Particles*, A. Septier, ed. (1967) Academic Press
- [2] L.H.Harwood, *et.al.* IEEE Trans. Mag. **25** (1989) 1910
- [3] W.Tuzel, *et.al.* IEEE Trans. Mag. **25** (1989) 1914
- [4] K.Tsuchiya, *et.al.* Nucl.Inst.Meth. **206** (1983) 57
- [5] CEBAF Conceptual Design Report on Basic Experimental Equipment, April 1990
- [6] Jerry B.Marion, "Classical Electromagnetic Radiation", Academic Press (1965), pg.79
- [7] Leigh H.Harwood, CEBAF technical note TN 90-0199 (1990)
- [8] TOSCA version 5.5, Vector Fields, Inc. 1700 N. Farnsworth Ave., Aurora IL 60505
- [9] See for example, R.A.Early and J.K Cobb, "Calculations and Measurements for the SLAC SLC Positron Return Quadrupole Magnet", SLAC-PUB-4093 (1986)
- [10] P.A.Reeve, *et.al.* Nucl.Inst.Meth. **135** (1976) 459

Table 1: Longitudinal Granularity used in TOSCA Calculation

$z$ (cm)	Number of Divisions	Type
$0 \leq z \leq 35$	4	Quadratic
$35 \leq z \leq 50$	3	Quadratic
$50 \leq z \leq 65$	15	Quadratic
$65 \leq z \leq 70$	5	Quadratic
$70 \leq z \leq 85$	3	Quadratic
$85 \leq z \leq 170$	9	Linear

Table 2: Multipole Components Integrated From  $z = 0$  to " $\infty$ "

Integrated Quantity	B.C.: $\Phi = \text{constant}$				B.C.: $\partial\Phi/\partial z = 0$			
	Fit $B_{r,n}(r)$		Fit $\Phi_n(r)$		Fit $B_{r,n}(r)$		Fit $\Phi_n(r)$	
	All Data	Only $r \leq 38$	All Data	Only $r \leq 38$	All Data	Only $r \leq 38$	All Data	Only $r \leq 38$
$n = 2$ ( $T \cdot m$ )								
$b_{0,2}$	0.935	0.935	0.935	0.935	0.940	0.940	0.940	0.940
$B_{r,2}(43 \text{ cm})$	0.939		0.937		0.943		0.941	
$B_{r,2}(38 \text{ cm})$	0.828	0.828	0.828	0.828	0.832	0.832	0.832	0.832
$B_{r,2}(30 \text{ cm})$	0.653	0.653	0.653	0.653	0.656	0.656	0.656	0.656
$n = 6$ (% of $n = 2$ )								
$b_{0,6}$	-1.84	-0.89	-1.12	-1.20	-1.77	-0.74	-1.03	-1.11
$B_{r,6}(43 \text{ cm})$	-1.30		-1.24		-1.19		-1.15	
$B_{r,6}(38 \text{ cm})$	-0.79	-0.78	-0.73	-0.73	-0.72	-0.72	-0.67	-0.67
$B_{r,6}(30 \text{ cm})$	-0.28	-0.29	-0.28	-0.28	-0.25	-0.26	-0.26	-0.26
$n = 10$ (% of $n = 2$ )								
$b_{0,10}$	8.09	-11.34	0.84	1.50	8.24	-10.15	0.75	1.44
$B_{r,10}(43 \text{ cm})$	-0.130		0.238		-0.156		0.222	
$B_{r,10}(38 \text{ cm})$	0.149	0.146	0.105	0.075	0.134	0.130	0.096	0.066
$B_{r,10}(30 \text{ cm})$	0.018	0.025	0.015	0.014	0.017	0.023	0.014	0.013

## Figure Captions

1. Cross sectional view through the center of the magnet. The pole tip radius (i.e. the minimum distance from the centerline to a pole piece) is 43 cm. The inner cryostat wall limits the warm (i.e. useful) radius to 38 cm. The iron is 130 cm long and ends abruptly with no shaping.
2. Details of the mesh used in the  $r\theta$  plane for the TOSCA calculation.
3. Setup of the iron and superconducting coils used in the TOSCA calculation.
4. Radial fit to the data for the radial field components  $B_{r,n}(r, z = 0)$  determined with  $\Phi = \text{constant}$  boundary conditions. We show  $n = 2, 6, \text{ and } 10$ .
5. Same as Fig. 4 except for  $z = 70 \text{ cm}$
6. Detailed look at the determination of the quadrupole ( $n = 2$ ) component of the radial field as a function of  $z$ . The thick solid line is the field component at  $r = r_0 = 43 \text{ cm}$ , i.e.  $B_{r,2}(r_0, z)$ , determined from the fitted coefficients. Also plotted are the fitted coefficients  $b_{m,2}(z)$  for  $m = 0, 1, 2, \text{ and } 3$ . Note that the integrals of  $B_{r,2}(r_0, z)$  and  $b_{0,2}(z)$  are equal, while the integrals of the other  $b_{m,2}(z)$  are zero.
7. Comparison of the coefficient  $b_{1,2}(z)$  determined directly from radial fits to  $B_{r,2}(r, z)$  to the quantity  $(r_0^2/6)d^2b_{0,2}/dz^2$  where  $b_{0,2}(z)$  is determined from the same radial fits. These should be the same according to Eqn. 5
8. Multipole components of the radial field as a function of  $z$  for  $n = 2$ . This particular analysis was done by fitting the potential  $\Phi_2(r)$  (determined with " $\Phi = \text{constant}$ " boundary conditions) to Eqn. 2 and determining  $B_{r,2}$  using Eqn. 3 and Eqn. 4. These curves correspond to the three different radii, with the larger fields near the center at the larger radius. *Top*: Multipole component  $B_{r,2}(r, z)$  for  $r = 30, 38, \text{ and}$

43 cm. Bottom: Integrated multipole component  $\int_0^z B_{r,2}(r, z) dz$  for the same three radii.

9. Same as Fig. 8 but for  $n = 6$ .

10. Same as Fig. 8 but for  $n = 10$ .

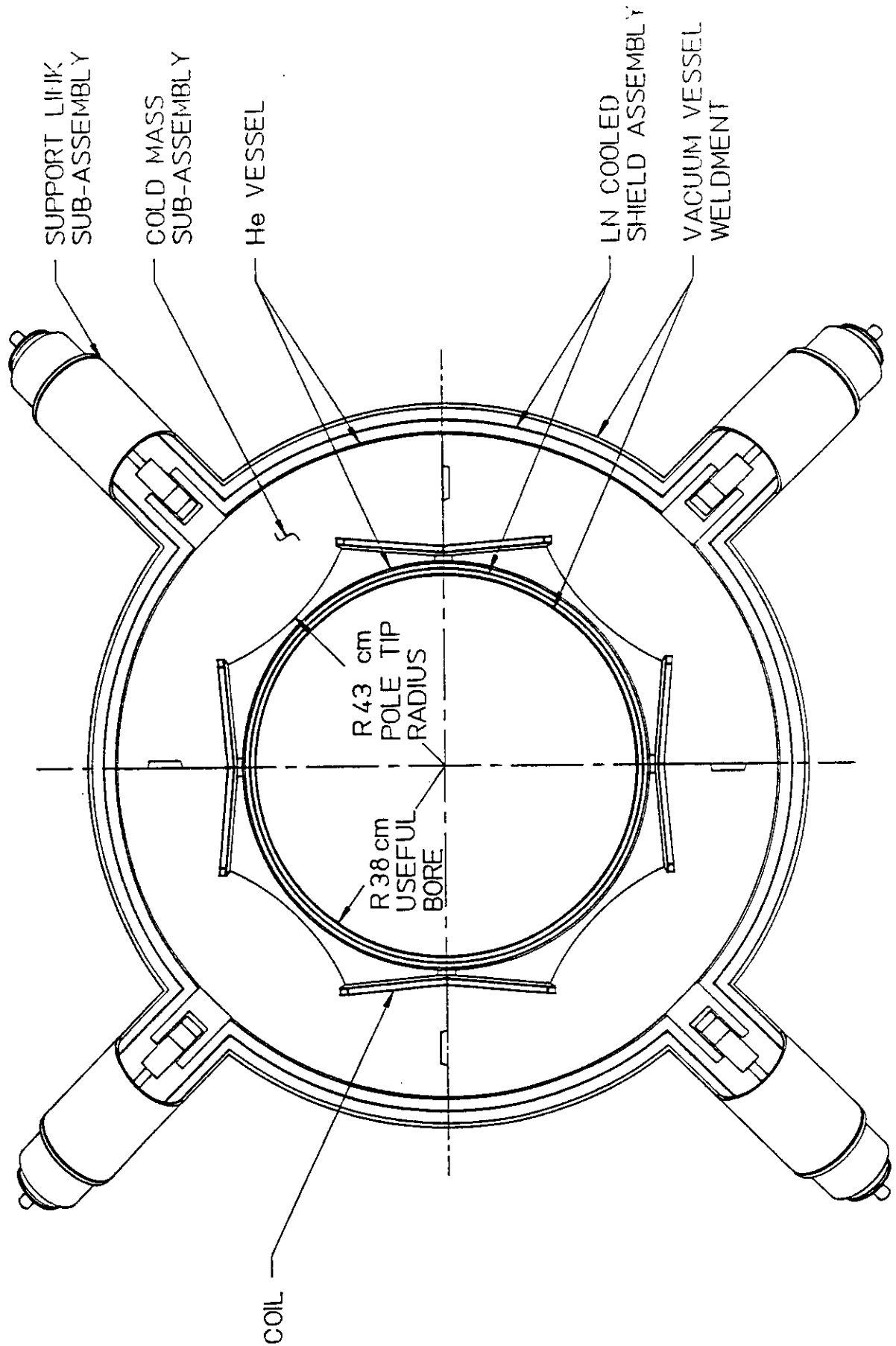


Figure 1

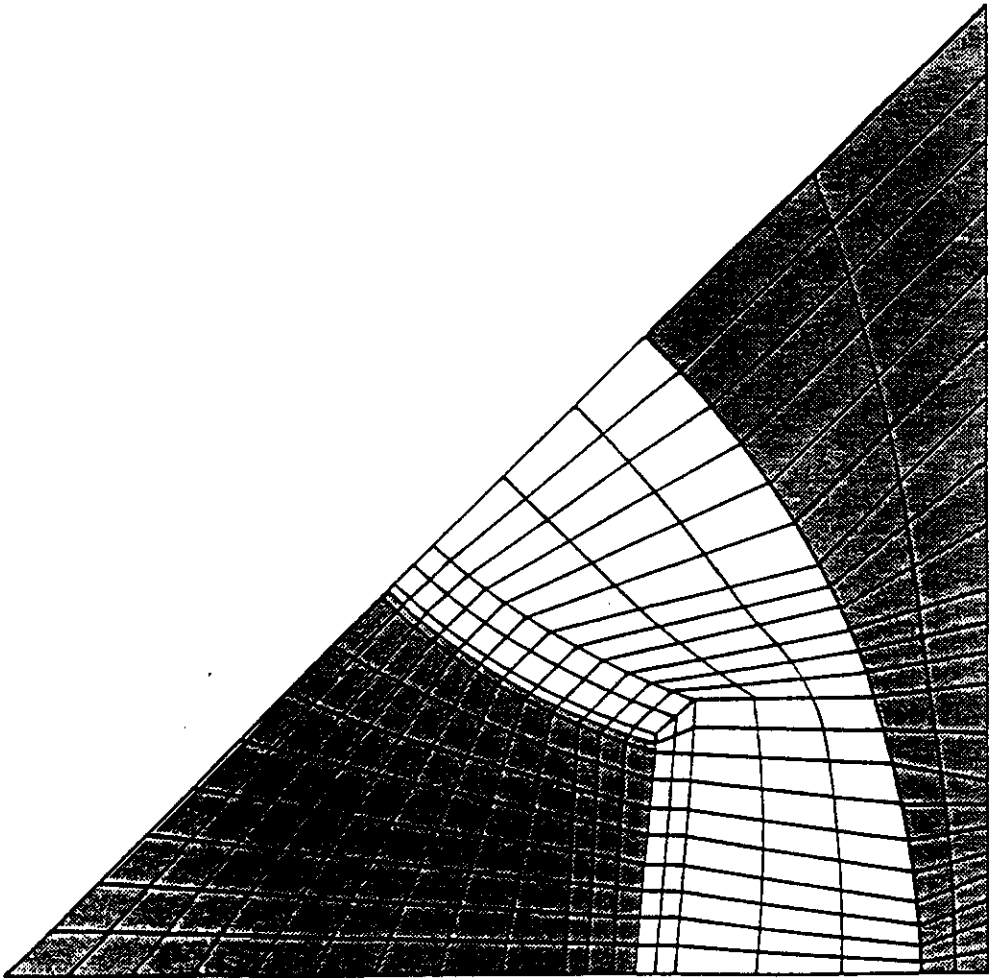


Figure 2

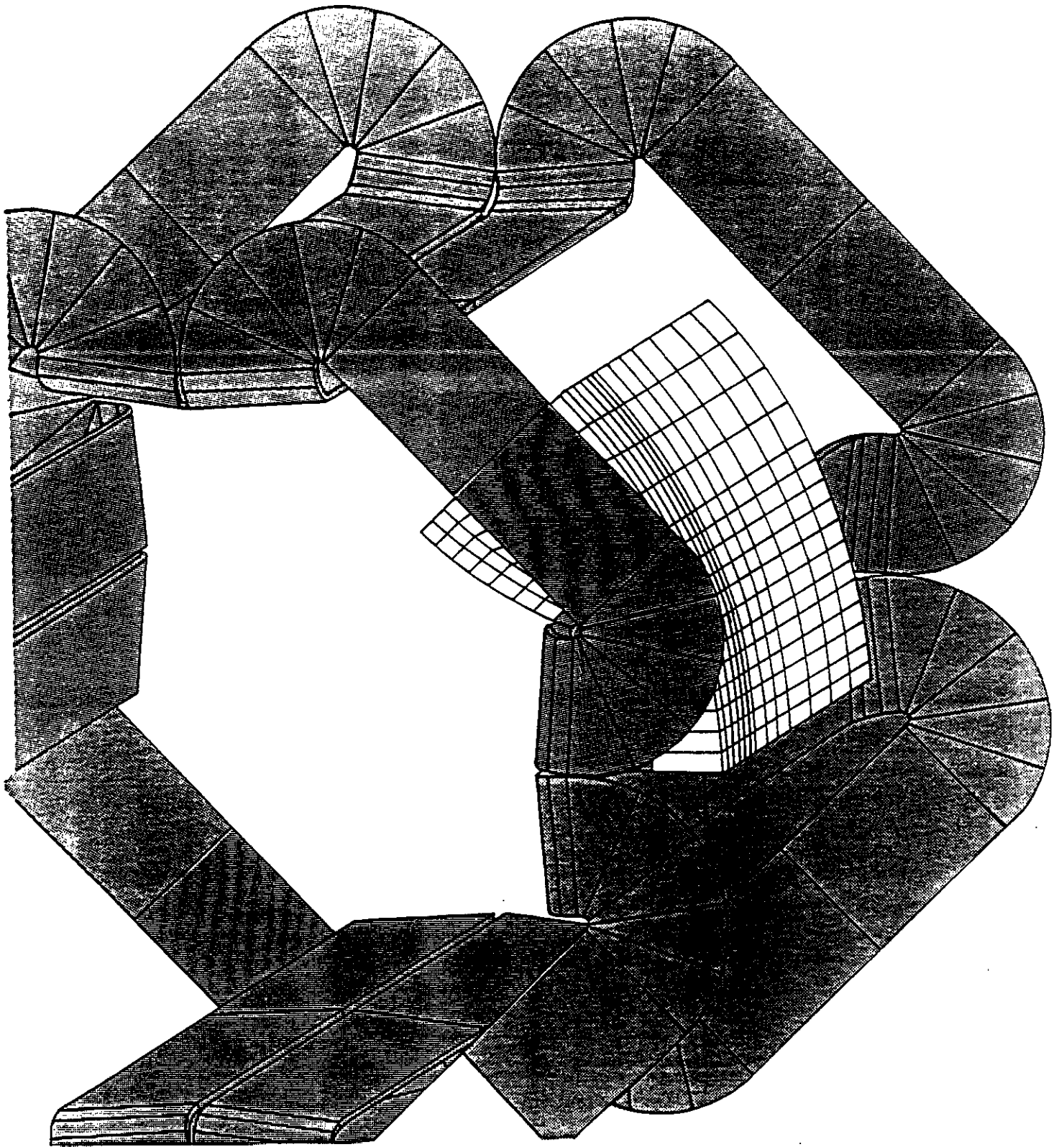


Figure 3

$z=0$

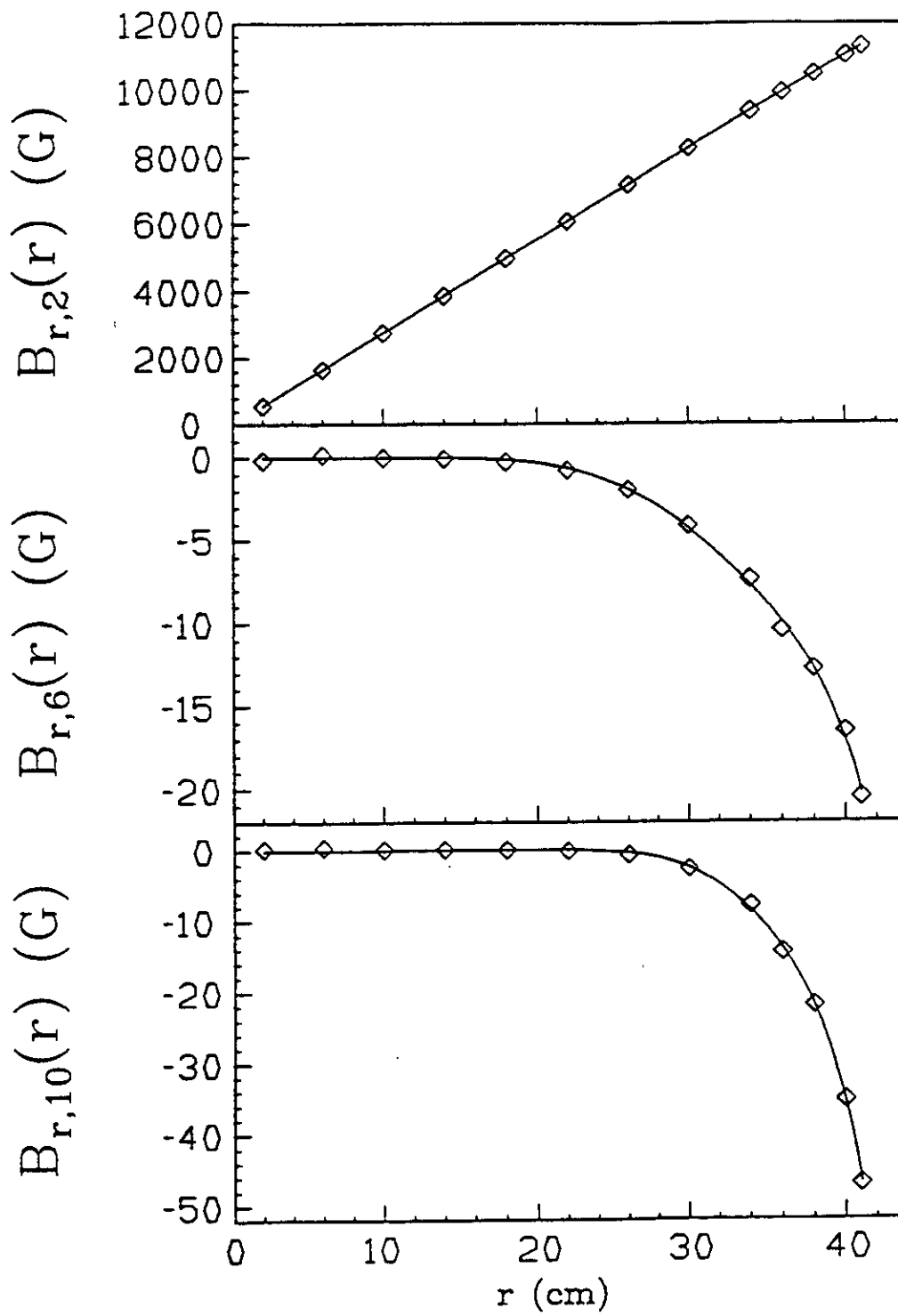


Figure 4

$z=70$  cm

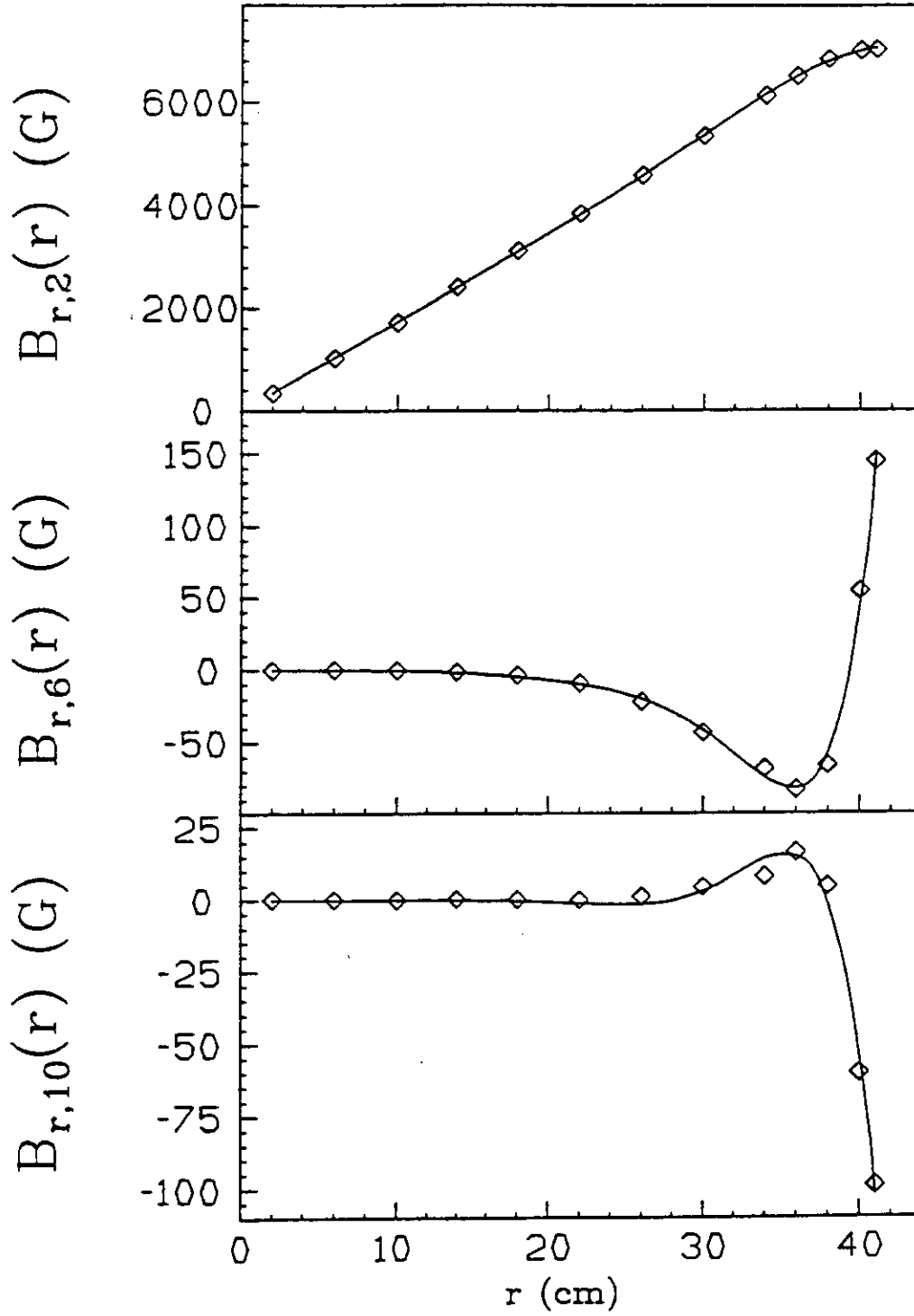


Figure 5

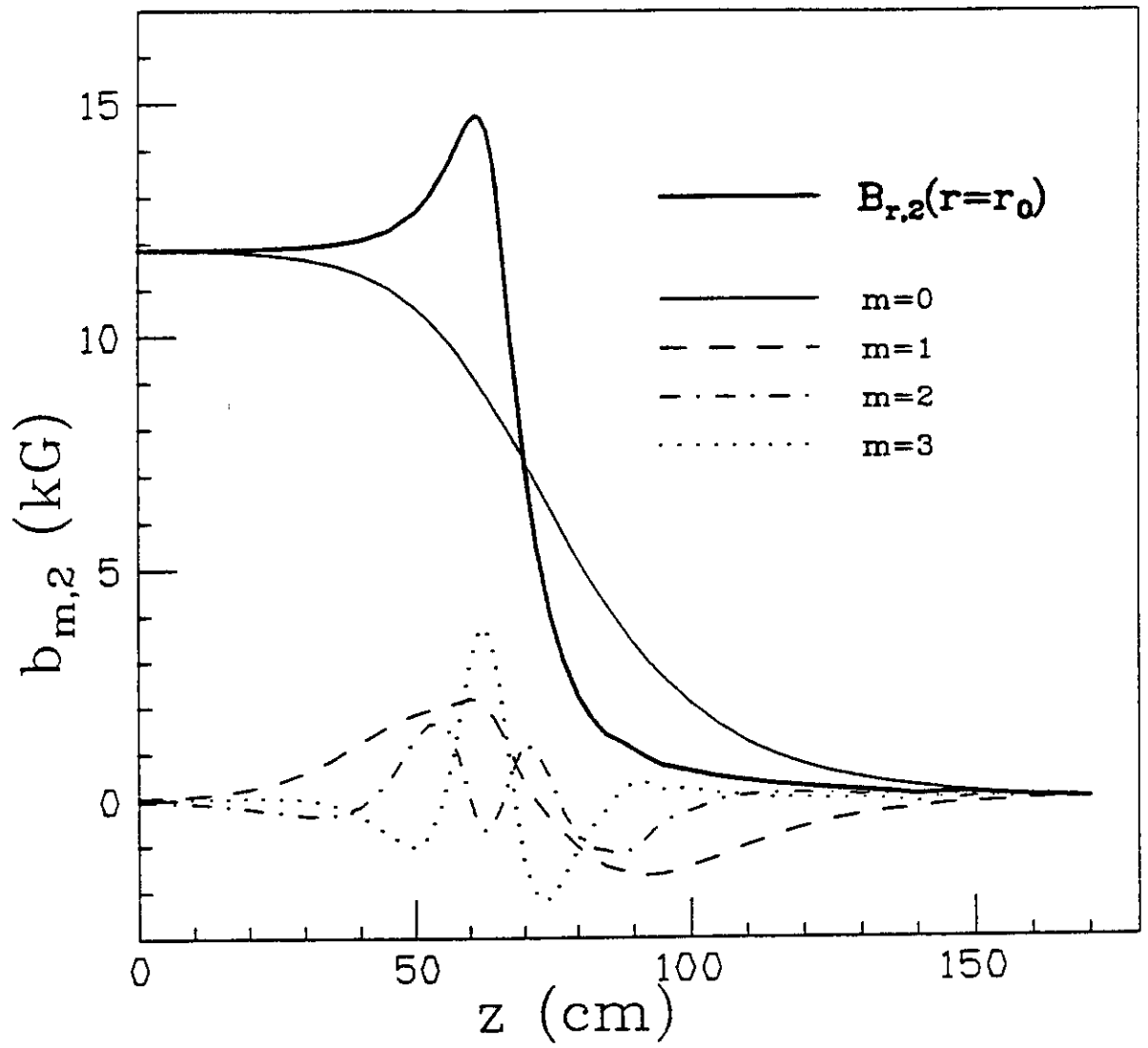


Figure 6

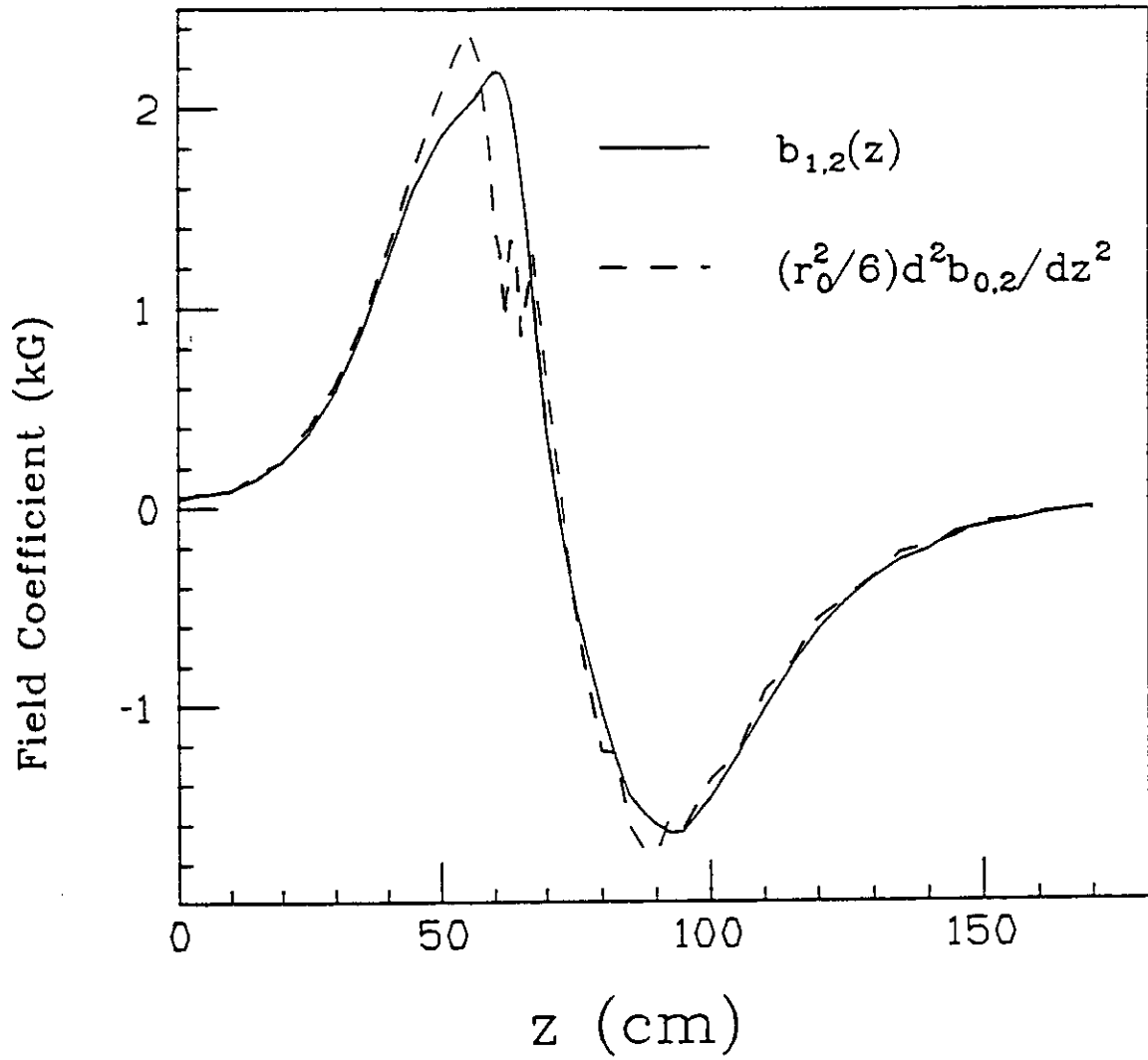


Figure 7

# n=2 Radial Fields

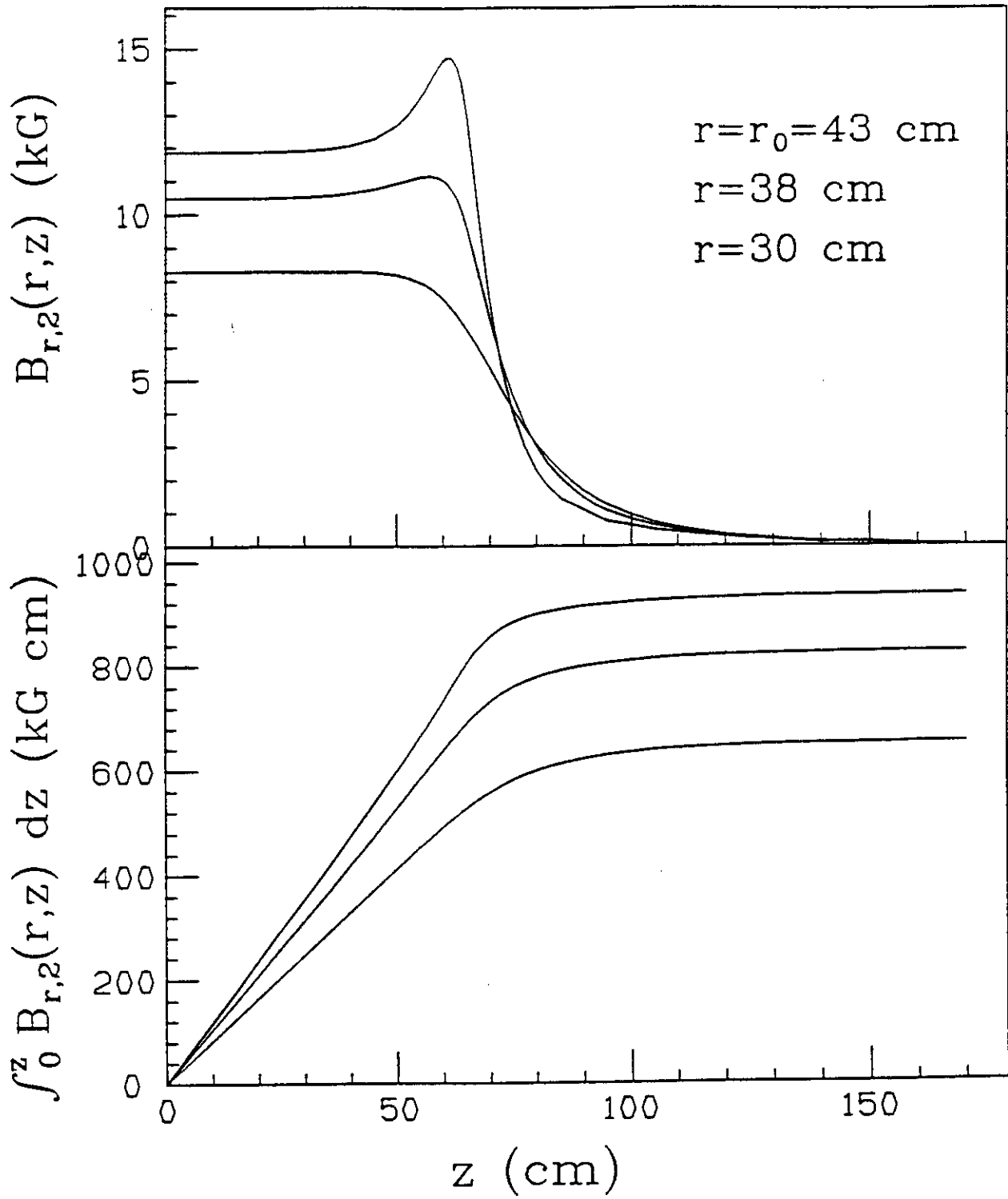


Figure 8

# n=6 Radial Fields

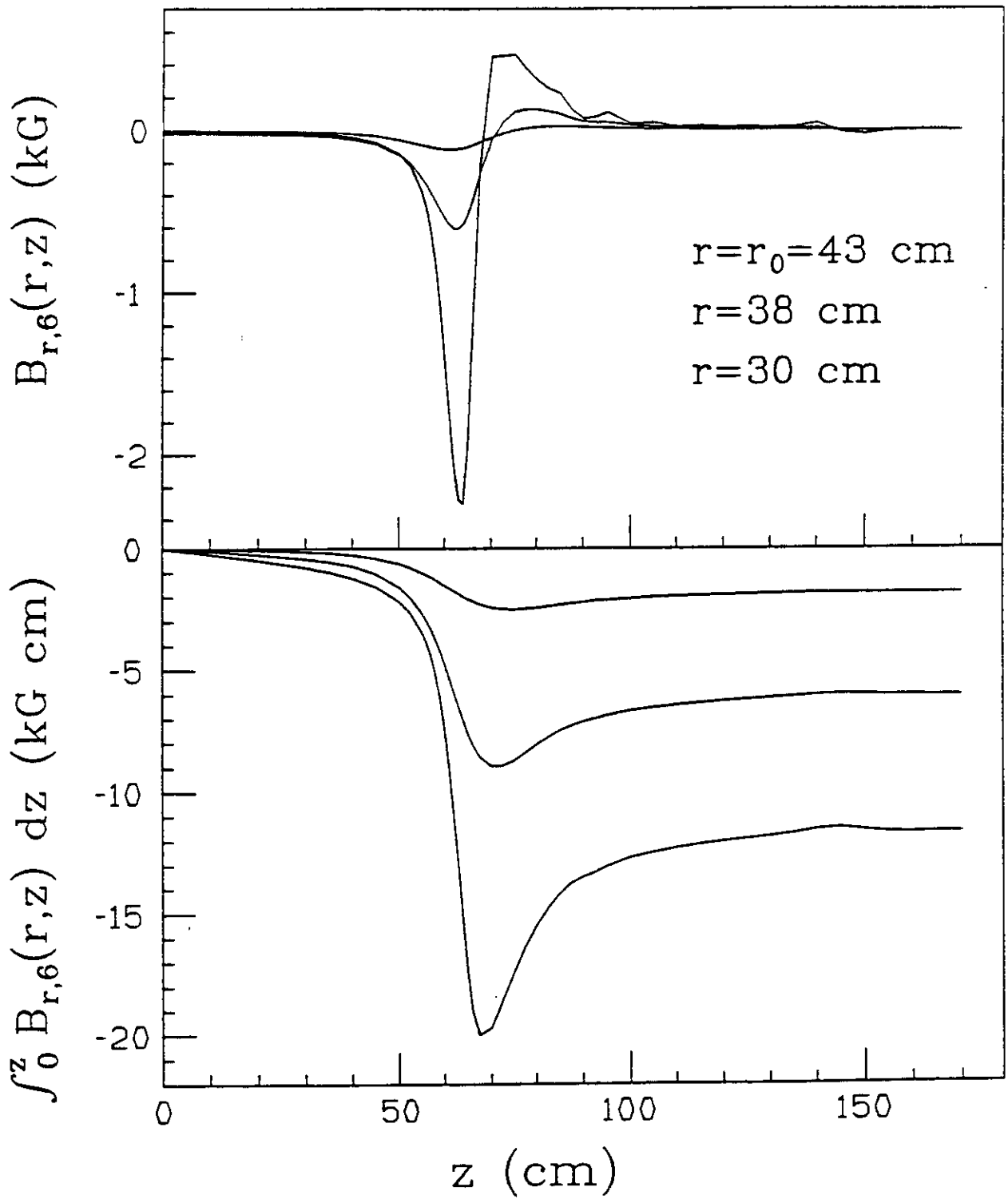


Figure 9

# n=10 Radial Fields

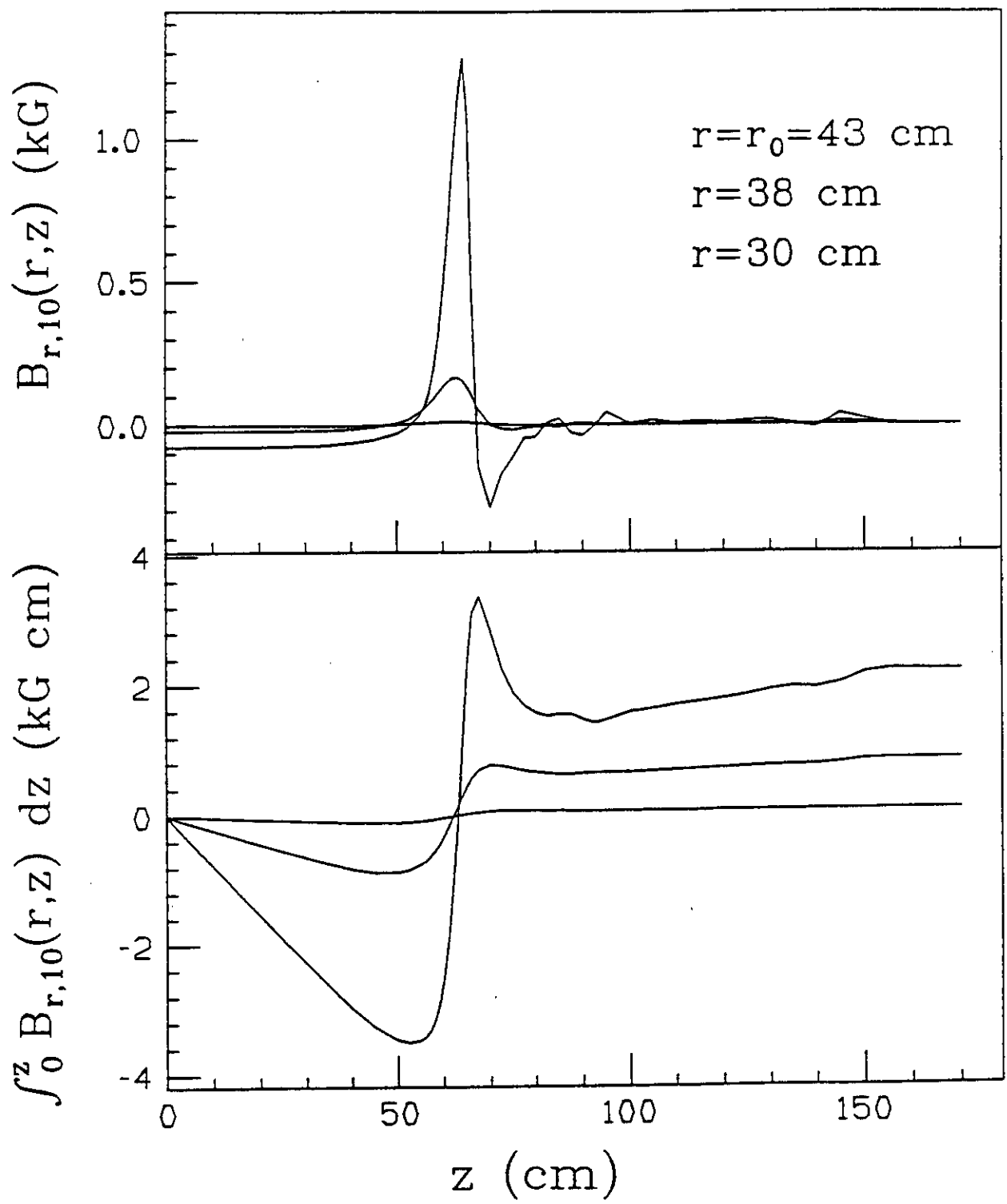


Figure 10